

Boosting photonic quantum computation with moderate nonlinearity

A. Pick,^{1,*} E. S. Matekole,² Z. Aqua,¹ G. Guendelman,¹ O. Firstenberg,³ J. P. Dowling,^{2,†} and B. Dayan¹

¹*Department of Chemical Physics, Weizmann Institute of Science, Rehovot 76100, Israel*

²*Department of Physics and Astronomy, Louisiana State University, Baton Rouge, LA 70803, USA*

³*Department of Physics, Weizmann Institute of Science, Rehovot 76100, Israel*

Photonic measurement-based quantum computation (MBQC) is a promising route towards fault-tolerant universal quantum computing. A central challenge in this effort is the huge overhead in the resources required for the construction of large photonic clusters using probabilistic linear-optics gates. Although strong single-photon nonlinearity ideally enables deterministic construction of such clusters, it is challenging to realise in a scalable way. Here we explore the prospects of using moderate nonlinearity (with conditional phase shifts smaller than π) to boost photonic quantum computing and significantly reduce its resources overhead. The key element in our scheme is a nonlinear router that preferentially directs photonic wavepackets to different output ports depending on their intensity. As a relevant example, we analyze the nonlinearity provided by Rydberg blockade in atomic ensembles, in which the trade-off between the nonlinearity and the accompanying loss is well understood. We present protocols for efficient Bell measurement and GHZ-state preparation – both key elements in the construction of cluster states, as well as for the CNOT gate and quantum factorization. Given the large number of entangling operations involved in fault-tolerant MBQC, the increase in success probability provided by our protocols already at moderate nonlinearities can result in a dramatic reduction in the required resources.

Photonic quantum computation is a leading platform in the effort towards fault-tolerant universal quantum computers [1–3]. It combines the paradigm of measurement-based quantum computation (MBQC) [4–10], where the computation is carried out by applying a sequence of measurements to clusters of entangled photons [11–13] with topological quantum error correction [14–19]. In particular, the promise of all-optical photonic quantum computation lies in the ability to entangle single photons into clusters using only linear-optics probabilistic operations [20–26]. The price, however, is a huge overhead: constructing a cluster of 10^7 photons (corresponding to ~ 1000 logical qubits, assuming $10^4 \times$ redundancy for error correction) with probabilistic gates may require 10^{12} input single photons [27].

One approach to tackle this challenge is efficient and strong interaction with single quantum emitters, such as atoms, ions, or quantum dots. Such coupling ideally enables deterministic construction of cluster states either by generation of a stream of entangled photons [28–31], or by entangling single photons via photon-atom quantum gates [32–37]. However, achieving strong interaction with single quantum emitters requires challenging optical structures, which are not straightforwardly scalable. A number of theoretical works explored the possibility of enhancing weak Kerr-type nonlinearities by classical driving fields to make them strong enough to support photonic quantum computation [38–47]. To be precise, we define nonlinearity as “strong” if it can provide a conditional phase shift $\varphi = \pi$; namely, a difference of π between twice the phase acquired by a single

photon in a mode, and the phase acquired by two photons in the same mode.

In contrast to previous studies, here we explore whether there is an intermediate regime between the linear optics and strong nonlinearity regimes in which moderate nonlinearity can provide a practical advantage. The motivation is that since fault-tolerant photonic quantum computation involves a large number of probabilistic gates [27], even a small improvement in the success probability per gate could amount to a dramatic reduction in the required resources. The reason for focusing on moderate nonlinearity is that attaining small phase shifts (e.g., $\pi/10$) typically requires significantly less resources than attaining π , and, accordingly, is accompanied by much lower costs, such as photon loss. Given the progress in photonic technologies and on-chip detection capabilities, we realistically assume in this study that the nonlinear medium itself will become the dominant source of loss in such a photonic device. In order to take this loss into account as accurately as possible, we consider below the very relevant and well-studied platform of electromagnetically-induced transparency with Rydberg atoms (Rydberg-EIT) [48, 49]. In these systems, the loss grows quadratically with the conditional phase shift φ (for small φ), which is eventually limited by the physical parameters of the Rydberg ensemble [50].

The key element in our protocols is a nonlinear router [51–53], realized by a Mach-Zehnder interferometer (MZI) with a nonlinear medium in both arms (Fig. 1). The conditional phase-shift acquired by two-photon pulses (photon pairs) in the nonlinear media causes the router to preferentially direct single photon pulses to one port and photon pairs to another. We use the router to obtain nonlinearity-

* adi.pick@weizmann.ac.il

† Deceased 5 June, 2020.

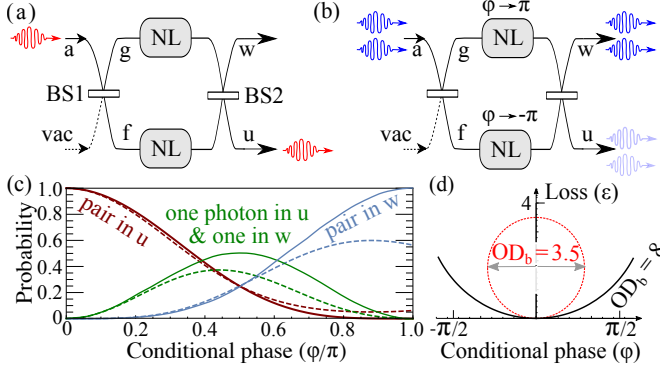


FIG. 1. **Nonlinear router:** (a) When a photon enters the interferometer in mode a , it leaves in mode u . (b) The interferometer contains a nonlinear medium (gray) in both arms. Photon pairs traveling through different arms acquire opposite conditional phases $\pm\varphi$ [Eq. (2)]. When $\varphi = \pi$, a pair that enters in mode a leaves in mode w . (c) Probabilities for detection outcomes for an incoming pair when $\varphi \in [0, \pi]$: both photons in u (brown), both in w (blue), and one in each mode (green). Solid lines show a loss-free model [Eq. (3)]. Dashed lines include nonlinear loss in Rydberg-EIT systems [τ in Eq. (6)] when $\text{OD}_b = 30$, which sets $\tau(\varphi)$ via Eq. (5) with $\varepsilon \equiv -\ln(1 - \tau)$ (d). The conditional phase-loss relation is a circle [50], shown for $\text{OD}_b = 3.5$ and 8 (red and black).

enhanced protocols for Bell-state measurement (BM) and for Greenberger–Horne–Zeiling (GHZ) state preparation (Figs. 2 and 3), which are key building blocks in MBQC [4]. As an application, we use these elements to construct protocols for a CNOT gate and quantum factorization (Fig. 4). By adding nonlinearity, our protocols outperform the linear methods, potentially reducing resource requirements for fault-tolerant photonic quantum computing by 2-3 orders of magnitude already at moderate nonlinearities.

Nonlinear router: As shown in Fig. 1(a), when single photons enter the MZI in mode a , they exit through port u , following the transformation rule [54]:

$$a^\dagger \xrightarrow{\text{BS1}} 1/\sqrt{2}(f^\dagger + ig^\dagger) \xrightarrow{\text{BS2}} u^\dagger. \quad (1)$$

The MZI contains a nonlinear atomic medium that induces opposite conditional phase shifts $\pm\varphi$ for photon pairs in each of its arms:

$$(f^\dagger)^2 \rightarrow e^{i\varphi}(f^\dagger)^2, \quad (g^\dagger)^2 \rightarrow e^{-i\varphi}(g^\dagger)^2. \quad (2)$$

As a result, photon pairs undergo the transformation

$$(a^\dagger)^2 \xrightarrow{\text{BS1}} \frac{1}{2} \left(e^{i\frac{\varphi}{2}} f^\dagger + ie^{-i\frac{\varphi}{2}} g^\dagger \right)^2 \xrightarrow{\text{BS2}} (w^\dagger \sin \frac{\varphi}{2} + u^\dagger \cos \frac{\varphi}{2})^2. \quad (3)$$

Consequently, the probability of routing pairs to the second output mode w increases monotonously with φ [Fig. 1(c)]. For $\varphi = \pi$, the nonlinear router deterministically separates pairs to a different port than single photons [Fig. 1(b)].

The effect of photon loss: While our protocol can be implemented using any type of nonlinearity, we focus on Rydberg-EIT systems to analyze loss. In such systems, once a photon generates a Rydberg excitation, the energy levels of the surrounding atoms (within the Rydberg-blockade radius) are shifted, violating the EIT conditions [55]. Consequently, any subsequent photon in this volume acquires a phase and suffers loss.

We model loss as the annihilation of a photon (in f or g) and the creation of a photon in an undetected mode (ℓ or k). Denoting the absorption probability by τ , a photon pair in the atomic medium follows the rule:

$$f^{\dagger 2} \rightarrow \sqrt{1 - \tau} e^{i\varphi} f^{\dagger 2} + \sqrt{\tau} f^\dagger \ell^\dagger \quad (4a)$$

$$g^{\dagger 2} \rightarrow \sqrt{1 - \tau} e^{-i\varphi} g^{\dagger 2} + \sqrt{\tau} g^\dagger k^\dagger. \quad (4b)$$

The conditional phase shift φ and absorption coefficient $\varepsilon \equiv -\ln(1 - \tau)$ follow the phase-loss circle [50]:

$$\varphi^2 + \left(\frac{\varepsilon}{2} - \frac{\text{OD}_b}{4}\right)^2 = \left(\frac{\text{OD}_b}{4}\right)^2, \quad (5)$$

where OD_b is the optical depth of the blockade volume – the core resource of nonlinearity in Rydberg-EIT systems [56]. As evident from Eq. (5) and Fig. 1(d), high OD_b enables large conditional phase shifts with low loss. In particular, $\text{OD}_b > 4\pi$ is required for $\varphi = \pi$. The value $\text{OD}_b = 13$ has already been reached experimentally [57], and higher values have been predicted [58, 59]. Additionally, high total OD can be utilized to generate an effective cavity in the atomic medium with finesse $F \sim (\text{OD}/2)^{0.4}$ [50], leading to a phase-loss circle whose radius is F times larger, thereby enabling an effective OD_b of 100 or more. Using Eqs. (1, 4, 5), we obtain

$$a^{\dagger 2} \rightarrow \frac{\sqrt{1 - \tau(\varphi)}}{2} \left[\cos \varphi (w^{\dagger 2} - u^{\dagger 2}) - 2 \sin \varphi (w^\dagger u^\dagger) \right] - \frac{1}{2} (w^{\dagger 2} + u^{\dagger 2}) + \frac{\sqrt{\tau(\varphi)}}{2\sqrt{2}} [(w^\dagger + iu^\dagger)\ell^\dagger - (u^\dagger + iw^\dagger)k^\dagger]. \quad (6)$$

From Eq. (6), we calculate the probabilities for different outcomes of the MZI when including loss [Fig. 1(c)].

Equations (5–6) assume that the photon wavelength is tuned exactly on the EIT resonance, where the single-photon phase shift and loss are ideally zero. In the supplementary material (SM), we analyze the possibility of detuning from the EIT resonance to introduce a single-photon phase shift. This detuning can reduce the nonlinear loss (as indicated by a shift of the phase-loss circle in Fig. C1), but it is unavoidably accompanied by single-photon loss. We find that this tradeoff leads to a minor improvement in the performance of our protocols.

Nonlinear Bell-state measurement (BM): As a first application, we use the nonlinear router to improve linear BMs. A photonic qubit is defined as a single excitation in an arbitrary coherent combination of two non-overlapping optical modes. For convenience, here we use the linear polarization basis, yet our analysis is generally applicable to any other choice of optical modes, including dual-rail or even time-bins [61].

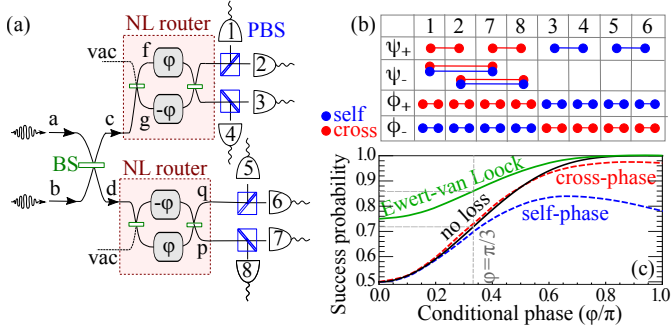


FIG. 2. **Nonlinear Bell measurement (BM):** Two photons are sent through a beam splitter (BS) and nonlinear routers before reaching detectors (1–8), which measure their joint state in the Bell basis. While $|\psi_{\pm}\rangle$ produce distinct final states, $|\phi_{\pm}\rangle$ can only be distinguished with nonlinearity. (b) Detector clicks for each Bell state, assuming $\varphi = \pi$ and neglecting loss. Blue (red) circles denote possible outcomes for self- (cross-) phase nonlinearity; e.g., with cross phase, $|\psi_+\rangle$ produces clicks in 1, 2 or 7, 8. (c) Success probability of a BM as a function of φ . Solid black curve neglects loss [P_{BM} from Eq. (8) with $\tau = 0$], as does the green curve, which shows the nonlinear enhancement of the Ewert-van Loock protocol [60], that includes four ancillary qubits [P_{EVL} from Eq. (A10)]. Blue (red) dashed curves include loss with self- (cross-) phase nonlinearities [Eqs. (8a–8b)] and $OD_b = 30$. Assuming linear loss is negligible, the cross-phase protocol outperforms the self-phase one, as it allows recovering of information on the Bell state when photons are lost. At $\varphi = \pi/3$, $P_{BM} = 0.72$ and $P_{EVL} = 0.86$.

In this basis, the photonic two-qubit Bell states are $|\psi_{\pm}\rangle = \frac{1}{\sqrt{2}}(a_H^\dagger b_V^\dagger \pm a_V^\dagger b_H^\dagger)|\text{vac}\rangle$ and $|\phi_{\pm}\rangle = \frac{1}{\sqrt{2}}(a_H^\dagger b_H^\dagger \pm a_V^\dagger b_V^\dagger)|\text{vac}\rangle$, where $|\text{vac}\rangle$ is the vacuum state. In a linear-optics BM, photons are sent through a balanced beam splitter (BS) [62]. Applying the BS transformation $a^\dagger \rightarrow \frac{1}{\sqrt{2}}(d^\dagger + ic^\dagger)$ and $b^\dagger \rightarrow \frac{1}{\sqrt{2}}(c^\dagger + id^\dagger)$, one finds

$$|\psi_-\rangle \xrightarrow{\text{BS}} \frac{1}{\sqrt{2}}(d_H^\dagger c_V^\dagger - c_H^\dagger d_V^\dagger)|\text{vac}\rangle, \quad (7a)$$

$$|\psi_+\rangle \xrightarrow{\text{BS}} \frac{i}{\sqrt{2}}(d_H^\dagger d_V^\dagger + c_H^\dagger c_V^\dagger)|\text{vac}\rangle, \quad (7b)$$

$$|\phi_{\pm}\rangle \xrightarrow{\text{BS}} \frac{i}{2\sqrt{2}}[(d_H^\dagger)^2 + (c_H^\dagger)^2 \pm ((d_V^\dagger)^2 + (c_V^\dagger)^2)]|\text{vac}\rangle. \quad (7c)$$

The states $|\psi_{\pm}\rangle$ lead to distinguishable outcomes; While $|\psi_-\rangle$ produces one photon in c and one in d , the state $|\psi_+\rangle$ produces an orthogonal pair in either c or d . In contrast, the states $|\phi_{\pm}\rangle$ produce a “bunched” pair in one of the four detectors and are, therefore, indistinguishable. Hence, when detectors are placed at the exit of the BS, the success probability of the BM is 50% [62]. To increase the success probability, we place nonlinear routers that help distinguish between $|\phi_{\pm}\rangle$ at the output of the BS [Fig. 2(a)]. When $\varphi = \pi$, all Bell states are distinguishable, as summarized in the table in Fig. 2(b).

To consider the effect of loss on our BM protocol, we analyze two types of nonlinear interactions: self-phase

nonlinearity, which takes place when two photons of the same polarization travel along the same arm of the MZI, and cross-phase nonlinearity, which takes place when two photons in the same arm are orthogonal. In the SM, we show that the success probability of our protocol is

$$P_{BM}^{(\text{self})} = 1 - \frac{1}{8} \left(\sqrt{1 - \tau(\varphi)} \cos \varphi + 1 \right)^2 - \frac{\tau(\varphi)}{4}, \quad (8a)$$

$$P_{BM}^{(\text{cross})} = 1 - \frac{1}{8} \left(\sqrt{1 - \tau(\varphi)} \cos \varphi + 1 \right)^2. \quad (8b)$$

The formulas are evaluated in Fig. 2(c). When neglecting loss (i.e., $\tau = 0$), Eqs. (8a,8b) are identical. Although self-phase modulation is more straightforwardly achievable in Rydberg-EIT systems [49, 63], cross-phase (also feasible [64]) has a higher success probability (by $\tau/4$). The reason for this difference is subtle. When writing the Bell states in the diagonal polarization basis, $\hat{x}_{\pm} \equiv \frac{1}{\sqrt{2}}(\hat{x}_H \pm \hat{x}_V)$, one finds that only $|\phi_-\rangle$ contains orthogonal photon pairs (hence affected by cross-phase nonlinearity), while both $|\phi_+\rangle$ and $|\psi_+\rangle$ contain identical photon pairs (affected by self-phase nonlinearity). Accordingly, assuming that the nonlinear-induced loss is indeed the dominant one, in cross-phase modulation a photon-loss event implies that the Bell state was $|\phi_-\rangle$ [65]. The possibility of recovering information out of null detection events is the only difference between the cross- and self-phase cases in the scope of this study.

Figure 2(c) also shows our nonlinear modification of the linear Ewert-van Loock protocol, that attains higher success probabilities at the cost of using four ancillary qubits [60, 66]. Details on the later protocol are given in the SM. A moderate conditional phase shift of $\pi/3$ (easily achievable using available setups [67]) improves the success probability of our protocol from 0.5 to 0.72, and that of the Ewert-van Loock protocol from 0.75 to 0.86. Evidently, in the presence of loss, the optimal operating point is at an intermediate phase $\varphi_{\text{opt}} < \pi$; it tends to π upon increasing OD_b , scaling as $\pi - \varphi_{\text{opt}} \propto OD_b^{-\alpha}$, with $\alpha = 1$ or $\frac{1}{3}$ for cross- or self-phase nonlinearity (Fig. D1).

Nonlinear GHZ-state preparation: Our protocol is shown in Fig. 3(a). Initially, two Bell states are prepared in $|\phi_+\rangle|\phi_+\rangle$. Then, one photon from each Bell pair is sent through a polarizing beam splitter (PBS1), which transmits horizontal and reflects vertical polarization. Then, the photons enter nonlinear routers. The photons may either leave PBS1 from different ports ($c_H^\dagger d_H^\dagger$ and $c_V^\dagger d_V^\dagger$) or through the same port ($c_H^\dagger c_V^\dagger$ and $d_H^\dagger d_V^\dagger$). In the former case, the photons leave the routers in modes u and p . Then, the photon in u undergoes a 45° rotation and a subsequent measurement of the rotated photon in the diagonal basis projects the surviving photons onto a GHZ state. This process is called “fusion type II” [21]. Our nonlinear scheme aims to “save” also photons that leave PBS1 through the same port. To this end, we use nonlinear routers that have the property that when $\varphi = \pi$, photons from $c_H^\dagger c_V^\dagger$ and $d_H^\dagger d_V^\dagger$ are routed into modes $w_H^\dagger w_V^\dagger$ and $q_H^\dagger q_V^\dagger$.

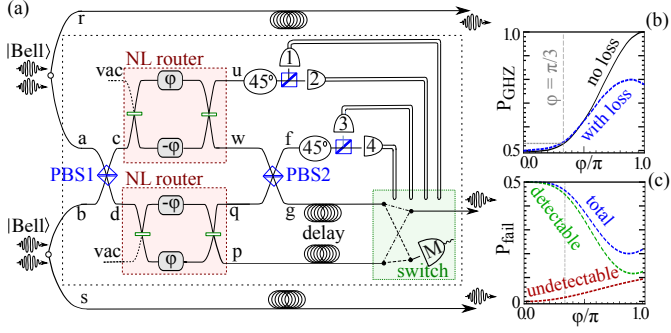


FIG. 3. **Nonlinear GHZ state generation:** (a) Two Bell pairs are prepared, and one photon from each pair is sent through PBS1. Two scenarios can produce a GHZ state: 1. When photons leave PBS1 through different ports and exit the routers in ports u and p . 2. When photons leave PBS1 through the same port and also exit the routers in w or q . Without loss, a single click in detectors 1–4 heralds success. The switch (green box) operates on photons in p and g and chooses which mode to output and which to measure; during its operation, photons travel in delay lines (coils). (b) Black-solid curve depicts the success probability when neglecting loss [$\tau = 0$ in Eq. (9)]. Blue-dashed curve includes loss, assuming $\text{OD}_b = 30$. At $\varphi = \pi/3$, we find $P_{\text{GHZ}} = 0.53$. (c) Probability for detectable (green), undetectable (red), and total (blue) failure in the presence of loss (with $\text{OD}_b = 30$).

(Here, φ may be achieved with cross-phase nonlinearity in the H/V basis or self-phase nonlinearity in the diagonal basis.) By sending these photons to PBS2, rotating the photon in mode f , and measuring the rotated photon in the diagonal basis, a GHZ state is produced.

By adding the probabilities for successful GHZ-state generation, either by “fusion type II” or by successful nonlinear routing, we obtain (see SM for details)

$$P_{\text{GHZ}} = \frac{1}{2} \left[1 + \frac{1}{4} \left(\sqrt{1 - \tau(\varphi)} \cos \varphi - 1 \right)^2 \right]. \quad (9)$$

P_{GHZ} as a function of φ is shown in Fig. 3(b). The result is the same regardless of using self- or cross-phase nonlinearity, since there is no way of extracting information from a photon-loss event. The optimal operating point is attained at $\varphi_{\text{opt}} < \pi$ and scales as $\pi - \varphi_{\text{opt}} \propto \text{OD}_b^{-1/3}$ with increasing OD_b (Fig. D1). When $\varphi = \pi/3$, we obtain $P_{\text{GHZ}} = 0.53$, while $\varphi = \pi/2$ produces $P_{\text{GHZ}} = 0.625$.

Our scheme requires a switch that selects to output mode g and measure p if there was a click in detectors 3 or 4, and vice versa if a click occurred in 1 or 2. During the switch operation, the photons travel in delay lines. When a photon is measured by the switch, it heralds failure since it implies that the output is empty. We distinguish between detectable failure – when either zero or two photons are detected – and undetectable loss – when a single click is obtained in detectors 1–4, but a photon is missing at the output. The probability of the latter terms is $\tau(\varphi)/8$, as plotted in Fig. 3(c).

CNOT and Factorization: In Ref. [4], Gottesman and Chuang (GC) present an optical-circuit implementation of the CNOT gate, which requires two GHZ states and three BMs [Fig. 4(a)]. Accordingly, the success probability of this protocol scales like $(P_{\text{GHZ}})^2 \times (P_{\text{BM}})^3$, being $1/2^5$ in the linear-optics case. When using our nonlinear elements, the success probability of the protocol increases by a factor of 3.32 at $\varphi = \pi/3$, as shown in Fig. 4(b). As CNOT is an elementary building block in most quantum protocols, this enhancement is a dramatic result. For example, the algorithm for quantum factorization of the number 15 from Ref. [68] requires two CNOT gates. Accordingly, our nonlinear protocols lead to an order-of-magnitude (11-fold) improvement in its success probability at $\varphi = \pi/3$ [Fig. 4(c)].

Discussion: We examined photonic quantum computation protocols in the intermediate regime between linear optics and strong nonlinearity at the single photon level, and presented efficient protocols for key elementary operations, including BM, GHZ-state generation, CNOT gate, and quantum factorization. Our results demonstrate the potential of moderate nonlinearity, which is achievable in a variety of platforms, using Rydberg-EIT systems [49, 63] as a relevant example. As photonic quantum computation, and fault-tolerant MBQC in particular, require very large number of elementary operations [27], any modest increase in the success probability of each operation is translated to a dramatic reduction in the required resources. For example, a conditional phase shift of $\varphi = \pi/3$, which in our scheme increases the success probability of ancilla-assisted BM from 0.75 to 0.86, and of GHZ-state preparation from 0.5 to 0.53 [69], is translated into two orders

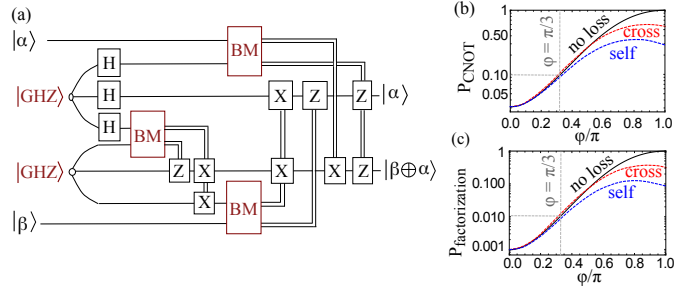


FIG. 4. **Nonlinear CNOT and quantum factorization:** (a) The Gottesman-Chuang linear CNOT gate [4]. The gate requires three BMs, two GHZ states and single-qubit Pauli (X, Z) and Hadamard (H) rotations. (b) Success probability (log scale) of the CNOT gate, using our nonlinear protocol (with BMs and GHZs from Figs. 2-3). Black-solid curve neglects loss, while blue (red) curves include loss using (self-) cross-phase nonlinearities with $\text{OD}_b = 30$. (c) Success probability (log scale) of quantum factorization of the number 15, using a protocol that requires two C-NOT gates [68], with the same building blocks and curve labels as in (b). For $\varphi = \pi/3$, the success probabilities of CNOT and quantum factorization increase by factors of 3.32 and 11 respectively.

of magnitude reduction in resources after 35 entangling operations, and three orders of magnitude improvement at 50 gates. With the recent developments in interacting atomic ensembles with integrated photonics [70–77], few-photon nonlinearity on chip-scale devices is becoming feasible, making protocols that rely on moderate nonlinearities a promising new platform for photonic quantum information processing.

Acknowledgment. The authors thank Ephraim Shahmoon, Serge Rosenblum, and Ran Finkelstein for helpful discussions. AP acknowledges support of the Koshland Foundation. BD and OF acknowledge support from the Israeli Science Foundation. BD and JPD are supported by Binational Science Foundation. BD is also supported by the Minerva Foundation, IMOD (OR RISHON), and a research grant from Dr. Saul Unter. OF is also supported by the European Research Council starting investigator grant QPHOTONICS 678674. ESM acknowledges the support of the US Air Force Office of Scientific Research.

SUPPLEMENTARY MATERIAL

TABLE OF CONTENTS

- A. Nonlinear Bell measurement
 - A1. Protocols with self- and cross-phase nonlinearity.
 - A2. Protocols with ancillas.
- B. Nonlinear GHZ-state preparation.
- C. Introducing single-photon phase shifts
 - C1. Nonlinear router
 - C2. Nonlinear Bell measurement.
 - C3. Nonlinear GHZ-state generation.
- D. Selecting optimal phase shifts.

A: Nonlinear Bell measurement

1. Protocols with self- and cross-phase nonlinearity

In this section, we provide calculation details for the success probability of a nonlinear Bell measurement (BM). The formulas we obtain are plotted in Fig. 2(b) in the text. First, rewrite Eq. (7) in the diagonal basis

$$\begin{aligned}
 |\psi_+\rangle &\xrightarrow{\text{BS}} \frac{i}{2\sqrt{2}}[(c_+^\dagger)^2 - (c_-^\dagger)^2 + (d_+^\dagger)^2 - (d_-^\dagger)^2]|\text{vac}\rangle \\
 |\phi_+\rangle &\xrightarrow{\text{BS}} \frac{i}{2\sqrt{2}}[(c_+^\dagger)^2 + (c_-^\dagger)^2 + (d_+^\dagger)^2 + (d_-^\dagger)^2]|\text{vac}\rangle \\
 |\phi_-\rangle &\xrightarrow{\text{BS}} \frac{i}{\sqrt{2}}[c_+^\dagger c_-^\dagger + d_+^\dagger d_-^\dagger]|\text{vac}\rangle.
 \end{aligned} \tag{A.1}$$

To trace the evolution of the states as they traverse the setup, we invoke the beam-splitter (BS) transformation

$$\begin{aligned}
 c^\dagger &\rightarrow \frac{1}{\sqrt{2}}(f^\dagger + ig^\dagger) \\
 f^\dagger &\rightarrow \frac{1}{\sqrt{2}}(w^\dagger + iu^\dagger) \\
 g^\dagger &\rightarrow \frac{1}{\sqrt{2}}(u^\dagger + iw^\dagger).
 \end{aligned} \tag{A.2}$$

We present two ways to implement the nonlinearity: using self- and cross-phase nonlinearity. When using cross-phase nonlinearity, an orthogonal pair transforms as

$$\begin{aligned}
 f_+^\dagger f_-^\dagger &\rightarrow \sqrt{1-\tau} e^{i\varphi} f_+^\dagger f_-^\dagger + \sqrt{\frac{\tau}{2}}(f_+^\dagger \ell_-^\dagger + f_-^\dagger \ell_+^\dagger), \\
 g_+^\dagger g_-^\dagger &\rightarrow \sqrt{1-\tau} e^{-i\varphi} g_+^\dagger g_-^\dagger + \sqrt{\frac{\tau}{2}}(g_+^\dagger k_-^\dagger + g_-^\dagger k_+^\dagger)
 \end{aligned} \tag{A.3}$$

With self-phase nonlinearity, identical photons obey the transformation rule

$$(f_\pm^\dagger)^2 \rightarrow \sqrt{1-\tau} e^{i\varphi} (f_\pm^\dagger)^2 + \sqrt{\tau} f_\pm^\dagger \ell_\pm^\dagger \tag{A.4}$$

$$(g_\pm^\dagger)^2 \rightarrow \sqrt{1-\tau} e^{i\varphi} (g_\pm^\dagger)^2 + \sqrt{\tau} g_\pm^\dagger k_\pm^\dagger \tag{A.5}$$

By using Eqs. (A.1–A.3), we obtain the transformation rule for the creation operators after traversing the interferometer. In the case of cross-phase nonlinearity, the cross terms transform as:

$$\begin{aligned}
 c_+^\dagger c_-^\dagger &\rightarrow \frac{\sqrt{1-\tau} \cos \varphi - 1}{2} w_+^\dagger w_-^\dagger - \frac{\sqrt{1-\tau} \cos \varphi + 1}{2} u_+^\dagger u_-^\dagger - \\
 &\sum_{\mu\nu=\pm} \left\{ \sqrt{1-\tau} \sin \varphi w_\mu^\dagger u_\nu^\dagger - \frac{\sqrt{\tau}}{2\sqrt{2}} [(w_\mu^\dagger + iu_\mu^\dagger) l_\nu^\dagger - (u_\nu^\dagger + iw_\nu^\dagger) k_\mu^\dagger] \right\}
 \end{aligned} \tag{A.6}$$

generalizing Eq. (6) in the main text. A similar transformation rule applies for the $d_+ d_-$ component of the wavefunction. Since $|\phi_-\rangle$ is the only state that contains cross terms, it is the only state affected by the nonlinearity. The BM fails only when both photons from $|\phi_-\rangle$ reach modes u_\pm . The failure probability is found by collecting the terms proportional to $u_+^\dagger u_-^\dagger$. We find

$$P_{\text{BM}}^{(\text{cross})} = 1 - \frac{1}{8} \left(\sqrt{1-\tau(\varphi)} \cos \varphi + 1 \right)^2. \tag{A.7}$$

In a similar manner, for self-phase nonlinearity, we use Eq. (A.5) and obtain

$$\begin{aligned}
 (c_\pm^\dagger)^2 &\rightarrow \frac{\sqrt{1-\tau} \cos \varphi - 1}{2} (w_\pm^\dagger)^2 - \frac{\sqrt{1-\tau} \cos \varphi + 1}{2} (u_\pm^\dagger)^2 - \\
 &\sqrt{1-\tau} \sin \varphi w_\pm^\dagger u_\pm^\dagger + \frac{\sqrt{\tau}}{2\sqrt{2}} [(w_\pm^\dagger + iu_\pm^\dagger) l_\pm^\dagger - (u_\pm^\dagger + iw_\pm^\dagger) k_\pm^\dagger]
 \end{aligned} \tag{A.8}$$

Both the states $|\phi_+\rangle$ and $|\psi_+\rangle$ are affected by the nonlinearity in this case, since both contain identical photon pairs [see Eq. (A.1)]. However, whenever two photons are detected, $|\phi_+\rangle$ is distinguishable from the remaining states because it is the only state that produces a

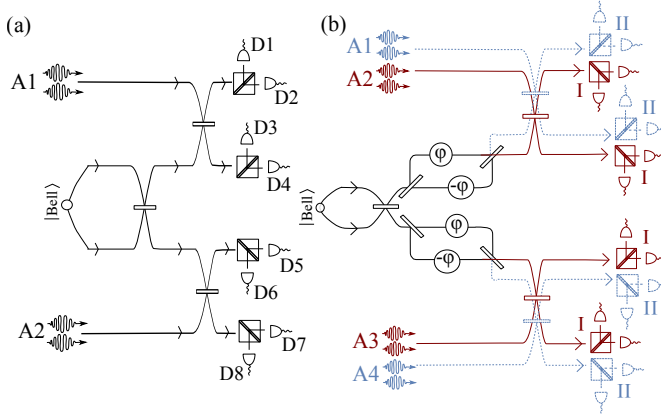


FIG. A.1. (a) Bell-state measurement using four ancillary qubits prepared in $\frac{1}{2}[(a_H^\dagger)^2 + (a_V^\dagger)^2]|\text{vac}\rangle$. A Bell state is sent through the device, and the final measurement can determine the input state with success probability of 75%. (b) By introducing nonlinear routers (and additional ancillas and detectors), the success probability increases, and reaches 100% for π conditional phase shifts, as shown by the green line in Fig. 2(b) in the main text.

pair of orthogonal photons either in the upper detectors (1–4) or in the lower detectors (5–8). Therefore, when both photons reach the detectors, only the cases where both photons from $|\psi_+\rangle$ are routed into $u_+^\dagger u_-^\dagger$ lead to failure. Photon loss also leads to failure of the BM. Both $|\phi_+\rangle$ and $|\psi_+\rangle$ can experience loss, and the final states in that case are indistinguishable. Given that the initial state is $|\psi_+\rangle$ or $|\phi_+\rangle$, the probability for loss is $\pi/2$. Therefore, the overall success probability becomes

$$P_{\text{BM}}^{(\text{self})} = 1 - \frac{1}{8} \left(\sqrt{1 - \tau(\varphi)} \cos \varphi + 1 \right)^2 - \frac{\tau(\varphi)}{4}, \quad (\text{A.9})$$

where the last term corresponds to indistinguishability due to loss, that is absent in the case of cross phase [compare with Eq. (8) in the main text].

2. Protocols with ancillas

In the main text, we present a Bell measurement (BM) that uses conditional phase shifts to improve a linear method whose success probability is 50%. However, linear protocols that use ancillary photons may have higher success rates, with probability approaching 100%; the failure rate drops exponentially with the number of ancillary photons [66]. The green curve in Fig. 1 depicts the success rate of a refined nonlinear protocol, which is based on a linear method with two ancillary qubits and success probability of 75% [60]. The protocol is shown in Fig. A1.

The linear method, proposed independently by Grice and Ewert and van-Loock [60, 66], utilizes four additional photons prepared in $|A_i\rangle =$

$\frac{1}{2}[(a_{i,H}^\dagger)^2 + (a_{i,V}^\dagger)^2]|\text{vac}\rangle$, where the index $i = 1, 2$ enumerates the ancillas and $|\text{vac}\rangle$ is the vacuum of the ancillary modes. The protocol is shown in Fig. A.1(a) and we briefly revise the linear method before introducing our nonlinear modification. By using 8 detectors, the Bell state can be determined with success probability of 75%; ψ_\pm and ϕ_\pm differ in the parity of H and V polarized photons, since the parity is unaltered by the device. ψ_\pm can be distinguished since they differ in the number of photons that reach the upper detectors ($D1, \dots, D4$). Finally, ϕ_\pm can only be distinguished with probability 50% (instances where all detected photons have the same polarization can occur for both ϕ_+ and ϕ_- and lead to failure). By introducing two nonlinear routers, one in each output of the first beam splitter, we increase the probability to distinguish between ϕ_\pm . The setup is shown in Fig. A.1(b). The success probability of our nonlinear protocol (when neglecting loss) is

$$P_{\text{EVL}} = 1 - \frac{1}{16} (\cos \varphi + 1)^2. \quad (\text{A.10})$$

With a conditional phase shift of π , the BM becomes deterministic. Note, however, that the nonlinear setup requires four ancillary qubits and eight detectors (while the linear counterpart required only two ancilla qubits).

B: Nonlinear GHZ-state preparation

In the main text, we describe a nonlinear protocol for GHZ-state generation. In this section, we provide the details of the derivation. The protocol uses a resource of two Bell pairs,

$$|\psi\rangle = \frac{1}{2}(r_H^\dagger a_H^\dagger + r_V^\dagger a_V^\dagger)(s_H^\dagger b_H^\dagger + s_V^\dagger b_V^\dagger)|\text{vac}\rangle. \quad (\text{B.1})$$

Then, one photon from each pair is sent through a polarizing beam splitter (PBS) (which transmits H -polarized photons and reflects V photons) and the state becomes

$$|\psi\rangle \xrightarrow{\text{PBS1}} \frac{1}{2}(r_H^\dagger d_H^\dagger + i r_V^\dagger c_V^\dagger)(s_H^\dagger c_H^\dagger + i s_V^\dagger d_V^\dagger)|\text{vac}\rangle. \quad (\text{B.2})$$

This wavefunction contains two types of components: ones with single photons in each output arm of the PBS ($c_H^\dagger d_H^\dagger$ and $c_V^\dagger d_V^\dagger$) and others with both photons in the same arm ($c_H^\dagger c_V^\dagger$ and $d_H^\dagger d_V^\dagger$). The former type of terms lead to successful GHZ-state generation. They leave the routers through ports u or p . Then, the photon in u undergoes a 45° rotation, resulting in

$$\begin{aligned} \frac{1}{2}(r_H^\dagger s_H^\dagger c_H^\dagger d_H^\dagger - r_V^\dagger s_V^\dagger c_V^\dagger d_V^\dagger) &\xrightarrow{\text{MZI}} \frac{1}{2}(r_H^\dagger s_H^\dagger p_H^\dagger u_H^\dagger - r_V^\dagger s_V^\dagger p_V^\dagger u_V^\dagger) \\ &\xrightarrow{45^\circ} \frac{1}{2\sqrt{2}}[u_+^\dagger(r_H^\dagger s_H^\dagger p_H^\dagger - r_V^\dagger s_V^\dagger p_V^\dagger) + u_-^\dagger(r_H^\dagger s_H^\dagger p_H^\dagger + r_V^\dagger s_V^\dagger p_V^\dagger)]. \end{aligned} \quad (\text{B.3})$$

Therefore, a click in either u_+ or u_- projects the surviving photons onto a GHZ state. On the other hand,

wavefunction components with both photons in the same arm (containing $c_H^\dagger c_V^\dagger$ and $d_H^\dagger d_V^\dagger$) are routed into modes u, p or w, q with probabilities shown in Fig. 1(c). Only the case where both photons are routed into w or q leads to successful GHZ generation. This is because the latter transform as

$$\begin{aligned} & \frac{1}{2}(r_V^\dagger s_H^\dagger w_H^\dagger w_V^\dagger + r_H^\dagger s_V^\dagger q_H^\dagger q_V^\dagger) \xrightarrow{\text{PBS2}} \frac{i}{2}(r_V^\dagger s_H^\dagger g_H^\dagger f_V^\dagger + r_H^\dagger s_V^\dagger f_H^\dagger g_V^\dagger) \\ & \xrightarrow{45^\circ} \frac{i}{2\sqrt{2}}[f_+^\dagger(r_V^\dagger s_H^\dagger g_H^\dagger + r_H^\dagger s_V^\dagger g_V^\dagger) + f_-^\dagger(r_V^\dagger s_H^\dagger g_H^\dagger - r_H^\dagger s_V^\dagger g_V^\dagger)]. \end{aligned} \quad (\text{B.4})$$

By scrutinizing the terms in the second line of Eq. (B.4), one can see that a measurement of the photon in mode f in the diagonal basis projects the surviving photons onto a GHZ state.

C: Introducing single-photon phase shifts

1. Nonlinear router

In this appendix, we introduce single-photon phase shifts in order to achieve conditional phase shifts with reduced loss. Our conclusion is that in all applications studied in this paper, this trade-off between initial phase and loss leads to a minor improvement in the performance. We present detailed derivations in this section and plot the results in Fig. C.1.

In this section, we consider a nonzero detuning from the EIT resonance, such that a photon traveling acquires a linear phase shift φ_1 and experiences loss ε_1 . Once a photon generates a Rydberg excitation, a subsequent photon inside the blockade radius effectively experiences an ensemble of two-level atoms and acquires a phase shift φ_2 and loss ε_2 . When neglecting loss, this model produces the following transformation rules for the creation operators in the MZI [Fig. 1(a) in the main text]:

$$f^\dagger \rightarrow e^{i\varphi_1} f^\dagger, \quad g^\dagger \rightarrow e^{-i\varphi_1} g^\dagger \quad (\text{C.1})$$

$$f^{\dagger 2} \rightarrow e^{i(\varphi_1 + \varphi_2)} f^{\dagger 2}, \quad g^{\dagger 2} \rightarrow e^{-i(\varphi_1 + \varphi_2)} g^{\dagger 2}. \quad (\text{C.2})$$

Our motivation is that by introducing small negative φ_1 , one needs a smaller φ_2 to achieve the same conditional phase shift,

$$\varphi \equiv \varphi_2 - \varphi_1. \quad (\text{C.3})$$

Since the phase shifts and loss coefficients satisfy the circle relations [Eq. (C.12) below], we expect to reduce the total loss

$$\varepsilon \equiv \varepsilon_1 + \varepsilon_2. \quad (\text{C.4})$$

Once introducing $\varphi_1 \neq 0$, one must balance the MZI (by adding a linear phase shift to one of its arm) in order for single photons to exit deterministically through

one port. Revisiting Eq. (1) from the main text and introducing single-photon phase shifts, $e^{\pm i\varphi_1}$, and an additional phase shift of $e^{i\Delta}$ for mode f , we obtain

$$\begin{aligned} a^\dagger & \xrightarrow{\text{BS1}} \frac{1}{\sqrt{2}}(e^{i(\varphi_1 + \Delta)} f^\dagger + i e^{-i\varphi_1} g^\dagger) \xrightarrow{\Delta = -2\varphi_1} \\ & \frac{e^{-i\varphi_1}}{\sqrt{2}}(f^\dagger + i g^\dagger) \xrightarrow{\text{BS2}} e^{-i\varphi_1} u^\dagger. \end{aligned} \quad (\text{C.5})$$

With this choice of Δ , the MZI is balanced. Next, let us trace the propagation of a photon pair in the MZI. Revisiting Eq. (3), we find

$$\begin{aligned} (a^\dagger)^2 & \xrightarrow{\text{BS1}} \frac{1}{2} \left(e^{i\frac{\varphi_1 + \varphi_2 + \Delta}{2}} f^\dagger + i e^{-i\frac{\varphi_1 + \varphi_2}{2}} g^\dagger \right)^2 \xrightarrow{\Delta = -2\varphi_1} \\ & \frac{e^{-2i\varphi_1}}{2} \left(e^{i\frac{\varphi}{2}} f^\dagger + i e^{-i\frac{\varphi}{2}} g^\dagger \right)^2 \xrightarrow{\text{BS2}} e^{-2i\varphi_1} (w^\dagger \sin \frac{\varphi}{2} + u^\dagger \cos \frac{\varphi}{2})^2. \end{aligned} \quad (\text{C.6})$$

In the second line, we used the definition of φ [Eq. (C.3)].

Next, let us introduce loss. The transformation rule [Eq. (C.2)] is modified:

$$f^\dagger \rightarrow \sqrt{1 - \tau_1} e^{i\varphi_1} f^\dagger + \text{loss}, \quad (\text{C.7})$$

$$g^\dagger \rightarrow \sqrt{1 - \tau_1} e^{-i\varphi_1} g^\dagger + \text{loss}, \quad (\text{C.8})$$

$$f^{\dagger 2} \rightarrow \sqrt{(1 - \tau_1)(1 - \tau_2)} e^{i(\varphi_1 + \varphi_2)} f^{\dagger 2} + \text{loss}, \quad (\text{C.9})$$

$$g^{\dagger 2} \rightarrow \sqrt{(1 - \tau_1)(1 - \tau_2)} e^{-i(\varphi_1 + \varphi_2)} g^{\dagger 2} + \text{loss}. \quad (\text{C.10})$$

Tracing the propagation of photon pairs through the MZI, we find [generalizing Eq. (5) in the main text]

$$\begin{aligned} a^{\dagger 2} & \rightarrow \frac{\sqrt{(1 - \tau_1)(1 - \tau_2)}}{2} e^{-2i\varphi_1} \left[\cos \varphi (w^{\dagger 2} - u^{\dagger 2}) - 2 \sin \varphi (w^\dagger u^\dagger) \right] \\ & - \frac{(1 - \tau_1)}{2} e^{-2i\varphi_1} (w^{\dagger 2} + u^{\dagger 2}) + \text{loss}. \end{aligned} \quad (\text{C.11})$$

The acquired phase shifts and loss coefficients satisfy the circle relation:

$$\varphi_i^2 + \left(\frac{\text{OD}}{4} - \frac{\varepsilon_i}{2} \right)^2 = \left(\frac{\text{OD}}{4} \right)^2, \quad (\text{C.12})$$

for $i = 1, 2$, where $e^{-\varepsilon_i} = 1 - \tau_i$.

Equation (C.11) is used in Fig. 1(a) in the main text to compute the probability for a photon pair to exit in modes w, u or both when $\varphi_1 \neq 0$ (dotted curves). The probabilities can be expressed in terms of $\varphi_1, \varphi, \varepsilon_1$, and ε . We choose φ_1 and φ and express $\varepsilon_1(\varphi_1)$ using Eq. (C.12) and the overall loss, using

$$\varepsilon(\varphi, \varphi_1) = \varepsilon_1(\varphi_1) + \frac{\text{OD}}{2} \pm \sqrt{\left(\frac{\text{OD}}{2} \right)^2 - 4(\varphi + \varphi_1)^2}. \quad (\text{C.13})$$

2. Nonlinear Bell measurement

First, we consider self-phase nonlinearity. Introducing conditional phase shifts for identical photon pairs,

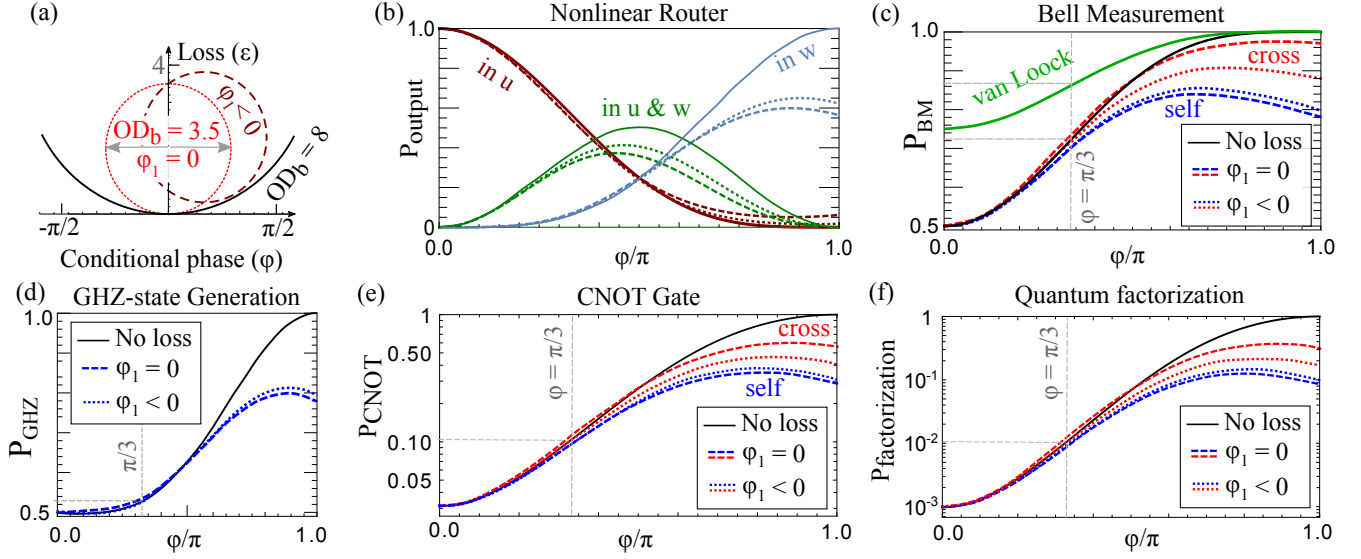


FIG. C.1. **Adding a single-photon phase shift, φ_1 , to reduce the nonlinear loss:** (a) Conditional phase-loss relation in Rydberg EIT systems, using Eq. (C.13). Same as Fig. 1(c), with the addition of the case $\varphi_1 = -0.5$, $OD_b = 3.5$ (brown-dashed curve). (b) Nonlinear router: Probabilities for detection outcomes for an incoming photon pair. Same as in Fig. 1(b), with the addition of the case $\varphi_1 = -\frac{\pi}{11}$, evaluated using Eq. (C.11) (dotted curves here and in all of the following subplots in this figure). This value of φ_1 was chosen to optimize the success probability and is used in all remaining subplots. (c-f) Success probabilities of a nonlinear BM, GHZ-states generation, CNOT gate, and quantum factorization as a function of φ . Same as Figs. 2(c), 3(b), 4(b,c), with the addition of the case $\varphi_1 < 0$.

the transformation rule for creation operators becomes

$$f_{\pm}^{\dagger 2} \rightarrow \sqrt{(1-\tau_1)(1-\tau_2)} e^{i(\varphi_1+\varphi_2)} f_{\pm}^{\dagger 2} + \text{loss}, \quad (\text{C.14})$$

$$f_{+}^{\dagger} f_{-}^{\dagger} \rightarrow (1-\tau_1) e^{2i\varphi_1} f_{+}^{\dagger} f_{-}^{\dagger} + \text{loss}. \quad (\text{C.15})$$

Recall that the states $|\psi_{-}\rangle$ and $|\phi_{-}\rangle$ do not contain identical photon pairs in the diagonal basis after the first BS [see Eq. (A.1)]. Therefore, these states can only encounter single-photon loss and the survival probability for each of these states is $(1-\tau_1)^2$. Conversely, the states $|\psi_{+}\rangle$ and $|\phi_{+}\rangle$ contain identical photon pairs. By summing the probability of the no-loss terms in Eq. (C.11), one finds that the survival probability for each of these states is $\frac{1}{2}[(1-\tau_1)^2 + (1-\tau_1)(1-\tau_2)]$. The interpretation of the last result is that either the photons survive two single-photon loss events (in an EIT medium) or they survive a single photon and a second-photon loss (in an effective two-level medium) event. The overall survival probability is

$$P_{\text{survive}}^{(\text{self})} = \frac{(1-\tau_1)^2}{2} + \frac{(1-\tau_1)(2-\tau_1-\tau_2)}{4}. \quad (\text{C.16})$$

Therefore, the success probability of a BM using self-phase nonlinearity is

$$P_{\text{BM}}^{(\text{self})} = P_{\text{survive}}^{(\text{self})} - \frac{1}{8} \left(\sqrt{(1-\tau_1)(1-\tau_2)} \cos \varphi + (1-\tau_1) \right)^2. \quad (\text{C.17})$$

Next, we discuss cross-phase nonlinearity. In this

case, the creation operators transform as

$$f_{+}^{\dagger} f_{-}^{\dagger} \rightarrow \sqrt{(1-\tau_1)(1-\tau_2)} e^{i(\varphi_1+\varphi_2)} f_{+}^{\dagger} f_{-}^{\dagger} + \text{loss}, \quad (\text{C.18})$$

$$f_{\pm}^{\dagger 2} \rightarrow (1-\tau_1) e^{2i\varphi_1} f_{\pm}^{\dagger 2} + \text{loss}. \quad (\text{C.19})$$

Revisiting Eq. (A.1), one learns that the states $|\psi_{\pm}\rangle$ and $|\phi_{+}\rangle$ do not contain orthogonal photon pairs in the diagonal basis, and only the state $|\phi_{-}\rangle$ does. Hence, the survival probability using cross-phase nonlinearity is

$$P_{\text{survive}}^{(\text{cross})} = \frac{3(1-\tau_1)^2}{4} + \frac{(1-\tau_1)(2-\tau_1-\tau_2)}{8}, \quad (\text{C.20})$$

and the success probability of a BM using cross-phase nonlinearity is

$$P_{\text{BM}}^{(\text{cross})} = P_{\text{survive}}^{(\text{cross})} - \frac{1}{8} \left(\sqrt{(1-\tau_1)(1-\tau_2)} \cos \varphi + (1-\tau_1) \right)^2. \quad (\text{C.21})$$

Equations (C.17) and (C.21) are used in Fig. 2(c) in the main text (dotted curves). While $P_{\text{BM}}^{(\text{self})}$ tends to the limit of Eq. (8) in the main text when $\varphi_1 \rightarrow 0$, the success probability in the case of cross-phase nonlinearity has a discontinuity at $\varphi_1 = 0$. The reason is that in the special case of $\varphi_1 = 0$ (i.e., allowing only nonlinear loss), photon loss can only occur when the initial state is $|\phi_{-}\rangle$. Therefore, loss does not produce an indeterminate outcome. However, as long as one allows linear loss, this property does not hold.

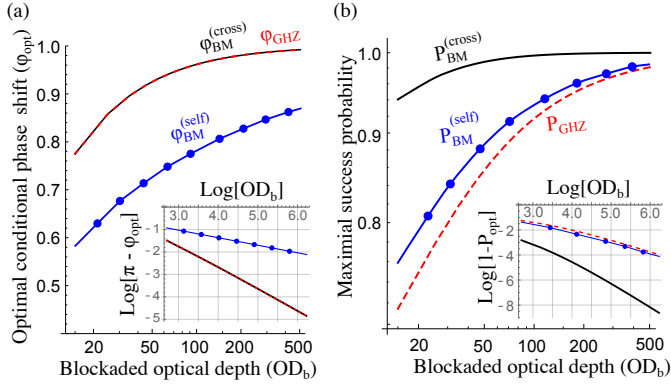


FIG. D.1. (a) Optimal phase shift as a function of the blockaded optical depth for BMs using cross- and self-phase nonlinearity (black solid and blue curve with circles) and for GHZ-state generation (red-dashed curve). (b) The success probabilities at the optimal phases shown in (a). The insets show the same data on a logarithmic scale.

3. Nonlinear GHZ-state generation

To compute the success probability of our protocol in the presence of $\varphi_1 \neq 0$, recall that there are two scenarios that produce a GHZ state: (i) When the photon pair leaves PBS1 through different ports and both photons reach the final detectors (avoiding absorption due to linear loss in the MZI), and (ii) When the photons leave PBS1 through the same port and, later, also leave the MZI in modes w or q . Adding the probabilities for

these scenarios, we obtain

$$P_{\text{GHZ}} = \frac{1}{2}(1 - \tau_1)^2 - \frac{1}{8} \left(\sqrt{(1 - \tau_1)(1 - \tau_2 \cos \varphi)} + (1 - \tau_1) \right)^2. \quad (\text{C.22})$$

Equation (C.22) is used in Fig. 3(b) in the main text.

D: Selecting optimal phase shifts

When examining the plots in the main text that show of the success probability versus φ , a surprising feature emerges: While one would naively expect that π phase shifts yield optimal results, it turns out that in all studied applications, the optimal phase is smaller than π . In Fig. D.1(a), we compute the optimal phase shift, φ_{opt} , as a function of the blockaded optical depth, OD_b , for BMs using cross- and self-phase nonlinearity and for GHZ-state generation (see black-solid, red-dashed, and blue curve with circles respectively). Figure D.1(b) shows the corresponding success probabilities at the optimal phase shifts from (a). The insets show the same data as the main plots on a logarithmic scale. One can see that at large optical depths ($\text{OD}_b > 50$), all curves in the insets are linear. We find that the optimal phases scale as $\varphi_{\text{opt}} - \pi \propto \text{OD}_b^\alpha$, where $\alpha = -1$ for BMs with cross-phase nonlinearity and GHZ-state preparation and $\alpha = -0.3$ for BMs with self-phase nonlinearity. The infidelity of our protocols scales as $1 - P_{\text{opt}} \propto \text{OD}_b^\alpha$, where $\alpha = -1.8$ for BMs with cross-phase nonlinearity while $\alpha = -0.9$ for BMs with self-phase and GHZ-state generation.

-
- [1] P. Kok, W. J. Munro, K. Nemoto, T. C. Ralph, J. P. Dowling, and G. J. Milburn, “Linear optical quantum computing with photonic qubits,” *Rev. Mod. Phys.* **79**, 135 (2007).
 - [2] J. L. O’Brien, A. Furusawa, and J. Vučković, “Photonic quantum technologies,” *Nat. Photonics* **3**, 687–695 (2009).
 - [3] T. Rudolph, “Why I am optimistic about the silicon-photonics route to quantum computing,” *APL Photonics* **2**, 030901 (2017).
 - [4] D. Gottesman and I. L. Chuang, “Demonstrating the viability of universal quantum computation using teleportation and single-qubit operations,” *Nature* **402**, 390–393 (1999).
 - [5] R. Raussendorf and H. J. Briegel, “A one-way quantum computer,” *Phys. Rev. Lett.* **86**, 5188 (2001).
 - [6] E. Knill, R. Laflamme, and G. J. Milburn, “A scheme for efficient quantum computation with linear optics,” *Nature* **409**, 46–52 (2001).
 - [7] M. A. Nielsen, “Quantum computation by measurement and quantum memory,” *Phys. Lett. A* **308**, 96–100 (2003).
 - [8] F. Verstraete and J. I. Cirac, “Valence-bond states for quantum computation,” *Phys. Rev. A* **70**, 060302(R) (2004).
 - [9] D. W. Leung, “Quantum computation by measurements,” *Int. J. Quantum Inf.* **2**, 33–43 (2004).
 - [10] H. J. Briegel, D. E. Browne, W. Dür, R. Raussendorf, and M. Van den Nest, “Measurement-based quantum computation,” *Nat. Phys.* **5**, 19–26 (2009).
 - [11] H. J. Briegel and R. Raussendorf, “Persistent entanglement in arrays of interacting particles,” *Phys. Rev. Lett.* **86**, 910 (2001).
 - [12] M. Hein, J. Eisert, and H. J. Briegel, “Multiparty entanglement in graph states,” *Phys. Rev. A* **69**, 062311 (2004).
 - [13] M. A. Nielsen, “Optical quantum computation using cluster states,” *Phys. Rev. Lett.* **93**, 040503 (2004).
 - [14] D. Gottesman, “Stabilizer codes and quantum error correction,” *arXiv: quant-ph/9705052* (1997).
 - [15] S. Bravyi and A. Kitaev, “Universal quantum computation with ideal Clifford gates and noisy ancillas,” *Phys. Rev. A* **71**, 022316 (2005).
 - [16] M. Varnava, D. E. Browne, and T. Rudolph, “Loss tolerance in one-way quantum computation via counter-

- factual error correction,” *Phys. Rev. Lett.* **97**, 120501 (2006).
- [17] C. M. Dawson, H. L. Haselgrove, and M. A. Nielsen, “Noise thresholds for optical quantum computers,” *Phys. Rev. Lett.* **96**, 020501 (2006).
 - [18] R. Raussendorf, J. Harrington, and K. Goyal, “Topological fault-tolerance in cluster state quantum computation,” *New J. of Phys.* **9**, 199 (2007).
 - [19] A. G. Fowler, M. Mariantoni, J. M. Martinis, and A. N. Cleland, “Surface codes: Towards practical large-scale quantum computation,” *Phys. Rev. A* **86**, 032324 (2012).
 - [20] A. Zeilinger, M. A. Horne, H. Weinfurter, and M. Żukowski, “Three-particle entanglements from two entangled pairs,” *Phys. Rev. Lett.* **78**, 3031 (1997).
 - [21] D. E. Browne and T. Rudolph, “Resource-efficient linear optical quantum computation,” *Phys. Rev. Lett.* **95**, 010501 (2005).
 - [22] C.-Y. Lu, X.-Q. Zhou, O. Gühne, W.-B. Gao, J. Zhang, Z.-S. Yuan, A. Goebel, T. Yang, and J.-W. Pan, “Experimental entanglement of six photons in graph states,” *Nat. Phys.* **3**, 91–95 (2007).
 - [23] K. Kielsing, T. Rudolph, and J. Eisert, “Percolation, renormalization, and quantum computing with nondeterministic gates,” *Phys. Rev. Lett.* **99**, 130501 (2007).
 - [24] P. J. Shadbolt, M. R. Verde, A. Peruzzo, A. Politi, A. Laing, M. Lobino, J. C. F. Matthews, M. G. Thompson, and J. L. O’Brien, “Generating, manipulating and measuring entanglement and mixture with a reconfigurable photonic circuit,” *Nat. Photonics* **6**, 45–49 (2012).
 - [25] X.-L. Wang, L.-K. Chen, W. Li, H.-L. Huang, C. Liu, C. Chen, Y.-H. Luo, Z.-E. Su, D. Wu, Z.-D. Li, H. Lu, Y. Hu, X. Jiang, C.-Z. Peng, L. Li, N.-L. Liu, Y. A. Chen, C. Y. Lu, and J.-W. Pan, “Experimental ten-photon entanglement,” *Phys. Rev. Lett.* **117**, 210502 (2016).
 - [26] D. Istrati, Y. Pilnyak, J. C. Loredó, C. Antón, N. Somaschi, P. Hilaire, H. Ollivier, M. Esmann, L. Cohen, L. Vidro, C. Millet, A. Lemaitre, I. Sagnes, A. Harouri, L. Lanco, P. Senellart, and H. S. Eisenberg, “Sequential generation of linear cluster states from a single photon emitter,” *Nature Communications* **11**, 1–8 (2020).
 - [27] Y. Li, P. C. Humphreys, G. J. Mendoza, and S. C. Benjamin, “Resource costs for fault-tolerant linear optical quantum computing,” *Phys. Rev. X* **5**, 041007 (2015).
 - [28] C. Schön, K. Hammerer, M. M. Wolf, J. I. Cirac, and E. Solano, “Sequential generation of matrix-product states in cavity QED,” *Phys. Rev. A* **75**, 032311 (2007).
 - [29] N. H. Lindner and T. Rudolph, “Proposal for pulsed on-demand sources of photonic cluster state strings,” *Phys. Rev. Lett.* **103**, 113602 (2009).
 - [30] I. Schwartz, D. Cogan, E. R. Schmidgall, Y. Don, L. Gantz, O. Kenneth, N. H. Lindner, and D. Gershoni, “Deterministic generation of a cluster state of entangled photons,” *Science* **354**, 434–437 (2016).
 - [31] H. Pichler, S. Choi, P. Zoller, and M. D. Lukin, “Universal photonic quantum computation via time-delayed feedback,” *Proc. Natl. Acad. Sci.* **114**, 11362–11367 (2017).
 - [32] L.-M. Duan and H. J. Kimble, “Scalable photonic quantum computation through cavity-assisted interactions,” *Phys. Rev. Lett.* **92**, 127902 (2004).
 - [33] A. Reiserer, N. Kalb, G. Rempe, and S. Ritter, “A quantum gate between a flying optical photon and a single trapped atom,” *Nature* **508**, 237–240 (2014).
 - [34] B. Hacker, S. Welte, G. Rempe, and S. Ritter, “A photon–photon quantum gate based on a single atom in an optical resonator,” *Nature* **536**, 193–196 (2016).
 - [35] S. Rosenblum, A. Borne, and B. Dayan, “Analysis of deterministic swapping of photonic and atomic states through single-photon Raman interaction,” *Phys. Rev. A* **95**, 033814 (2017).
 - [36] O. Bechler, A. Borne, S. Rosenblum, G. Guendelman, O. E. Mor, M. Netser, T. Ohana, Z. Aqua, N. Drucker, R. Finkelstein, Y. Lovsky, R. Bruch, D. Gurovich, E. Shafir, and B. Dayan, “A passive photon–atom qubit swap operation,” *Nat. Phys.* **14**, 996–1000 (2018).
 - [37] J. Borregaard, A. S. Sørensen, and P. Lodahl, “Quantum networks with deterministic spin–photon interfaces,” *Adv. Quantum Technol.* **2**, 1800091 (2019).
 - [38] W. J. Munro, K. Nemoto, and T. P. Spiller, “Weak nonlinearities: a new route to optical quantum computation,” *N. J. Phys.* **7**, 137 (2005).
 - [39] W. J. Munro, K. Nemoto, R. G. Beausoleil, and T. P. Spiller, “High-efficiency quantum-nondemolition single-photon-number-resolving detector,” *Phys. Rev. A* **71**, 033819 (2005).
 - [40] S. D. Barrett, P. Kok, K. Nemoto, R. G. Beausoleil, W. J. Munro, and T. P. Spiller, “Symmetry analyzer for nondestructive Bell-state detection using weak nonlinearities,” *Phys. Rev. A* **71**, 060302(R) (2005).
 - [41] S. G. R. Louis, K. Nemoto, W. J. Munro, and T. P. Spiller, “The efficiencies of generating cluster states with weak nonlinearities,” *N. J. Phys.* **9**, 193 (2007).
 - [42] K. Nemoto and W. J. Munro, “Nearly deterministic linear optical controlled-NOT gate,” *Phys. Rev. Lett.* **93**, 250502 (2004).
 - [43] K. Nemoto and W. J. Munro, “Universal quantum computation on the power of quantum non-demolition measurements,” *Phys. Lett. A* **344**, 104–110 (2005).
 - [44] M. G. A. Paris, M. B. Plenio, S. Bose, D. Jonathan, and G. M. D’ariano, “Optical Bell measurement by Fock filtering,” *Phys. Lett. A* **273**, 153–158 (2000).
 - [45] J. H. Shapiro, “Single-photon Kerr nonlinearities do not help quantum computation,” *Phys. Rev. A* **73**, 062305 (2006).
 - [46] J. H. Shapiro and M. Razavi, “Continuous-time cross-phase modulation and quantum computation,” *New J. Phys.* **9**, 16 (2007).
 - [47] J. Gea-Banacloche, “Impossibility of large phase shifts via the giant Kerr effect with single-photon wave packets,” *Phys. Rev. A* **81**, 043823 (2010).
 - [48] E. Distante, P. Farrera, A. Padrón-Brito, D. Paredes-Barato, G. Heinze, and H. De Riedmatten, “Storing single photons emitted by a quantum memory on a highly excited Rydberg state,” *Nat. Commun.* **8**, 1–6 (2017).
 - [49] D. Tiarks, S. Schmidt-Eberle, T. Stolz, G. Rempe, and S. Dürr, “A photon–photon quantum gate based on Rydberg interactions,” *Nat. Phys.* **15**, 124–126 (2019).
 - [50] O. Lahad and O. Firstenberg, “Induced cavities for photonic quantum gates,” *Phys. Rev. Lett.* **119**, 113601 (2017).
 - [51] S. Rosenblum, O. Bechler, I. Shomroni, Y. Lovsky, G. Guendelman, and B. Dayan, “Extraction of a sin-

- gle photon from an optical pulse,” *Nat. Photonics* **10**, 19–22 (2016).
- [52] T. G. Tiecke, J. D. Thompson, N. P. de Leon, L. R. Liu, V. Vuletić, and M. D. Lukin, “Nanophotonic quantum phase switch with a single atom,” *Nature* **508**, 241–244 (2014).
- [53] T. C. Ralph, I. Söllner, S. Mahmoodian, A. G. White, and P. Lodahl, “Photon sorting, efficient bell measurements, and a deterministic controlled-Z gate using a passive two-level nonlinearity,” *Phys. Rev. Lett.* **114**, 173603 (2015).
- [54] C. Gerry, P. Knight, and P. L. Knight, *Introductory Quantum Optics* (Cambridge university press, 2005).
- [55] A. V. Gorshkov, J. Otterbach, M. Fleischhauer, T. Pohl, and M. D. Lukin, “Photon-photon interactions via Rydberg blockade,” *Phys. Rev. Lett.* **107**, 133602 (2011).
- [56] There is a factor of 2 difference between our definition of ε and Ref. [50], since we refer to loss of modal amplitude and Ref. [50] refers to intensity loss.
- [57] C. Tresp, C. Zimmer, I. Mirgorodskiy, H. Gorniaczyk, A. Paris-Mandoki, and S. Hofferberth, “Single-photon absorber based on strongly interacting Rydberg atoms,” *Phys. Rev. Lett.* **117**, 223001 (2016).
- [58] S. Baur, D. Tiarks, G. Rempe, and S. Dürr, “Single-photon switch based on Rydberg blockade,” *Phys. Rev. Lett.* **112**, 073901 (2014).
- [59] A. Gaj, A. T. Krupp, J. B. Balewski, R. Löw, S. Hofferberth, and T. Pfau, “From molecular spectra to a density shift in dense Rydberg gases,” *Nat. Commun.* **5**, 1–5 (2014).
- [60] F. Ewert and P. van Loock, “3/4-efficient Bell measurement with passive linear optics and unentangled ancillae,” *Phys. Rev. Lett.* **113**, 140403 (2014).
- [61] While this is correct for self-phase nonlinearity, cross-phase nonlinear shifts require that the two optical modes will overlap spatially on the nonlinear medium.
- [62] S. L. Braunstein and A. Mann, “Measurement of the Bell operator and quantum teleportation,” *Phys. Rev. A* **51**, R1727 (1995).
- [63] O. Firstenberg, T. Peyronel, Q.-Y. Liang, A. V. Gorshkov, M. D. Lukin, and V. Vuletić, “Attractive photons in a quantum nonlinear medium,” *Nature* **502**, 71–75 (2013).
- [64] Cross-phase modulation could potentially be achieved in Rydberg atoms by coupling two photons to Rydberg states of opposite parity. Rydberg-state combinations can be chosen and enhanced using Förster resonance [78, 79].
- [65] In the SM, we include also the effect of single-photon loss in the atomic medium on the BM. In that case, all Bell states may experience loss. Consequently, the difference between $P_{\text{BM}}^{(\text{self})}$ and $P_{\text{BM}}^{(\text{cross})}$ becomes less pronounced [see Eqs. (C17) and (C21) and Fig. C1(c)].
- [66] W. P. Grice, “Arbitrarily complete Bell-state measurement using only linear optical elements,” *Phys. Rev. A* **84**, 042331 (2011).
- [67] Z.-Y. Liu, Y.-H. Chen, Y.-C. Chen, H.-Y. Lo, P.-J. Tsai, I. A. Yu, Y.-C. Chen, and Y.-F. Chen, “Large cross-phase modulations at the few-photon level,” *Phys. Rev. Lett.* **117**, 203601 (2016).
- [68] A. Politi, J. C. F. Matthews, and J. L. O’Brien, “Shor’s quantum factoring algorithm on a photonic chip,” *Science* **325**, 1221–1221 (2009).
- [69] At these small values of phase shifts the loss is negligible, so these estimates were obtained using the loss-free model.
- [70] L. Stern, B. Desiatov, I. Goykhman, and U. Levy, “Nanoscale light-matter interactions in atomic cladding waveguides,” *Nat. Commun.* **4**, 1–7 (2013).
- [71] M. Keil, O. Amit, S. Zhou, D. Groswasser, Y. Japha, and R. Folman, “Fifteen years of cold matter on the atom chip: promise, realizations, and prospects,” *J. Mod. Opt.* **63**, 1840–1885 (2016).
- [72] J. Kitching, “Chip-scale atomic devices,” *Appl. Phys. Rev.* **5**, 031302 (2018).
- [73] Y. Meng, A. Dureau, P. Schneeweiss, and A. Rauschenbeutel, “Near-ground-state cooling of atoms optically trapped 300 nm away from a hot surface,” *Phys. Rev. X* **8**, 031054 (2018).
- [74] N. V. Corzo, J. Raskop, A. Chandra, A. S. Sheremet, B. Gouraud, and J. Laurat, “Waveguide-coupled single collective excitation of atomic arrays,” *Nature* **566**, 359–362 (2019).
- [75] A. Johnson, M. Blaha, A. E. Ulanov, A. Rauschenbeutel, P. Schneeweiss, and J. Volz, “Observation of collective superstrong coupling of cold atoms to a 30-m long optical resonator,” *Phys. Rev. Lett.* **123**, 243602 (2019).
- [76] R. Finkelstein, G. Winer, D. Z. Koplovich, O. Arenfrid, T. Hoinkes, G. Guendelman, M. Netser, E. Poem, A. Rauschenbeutel, B. Dayan, and O. Firstenberg, “Super-extended nanofiber-guided field for coherent interaction with hot atoms,” *arXiv: 2010.08935* (2020).
- [77] X.-L. Pang, A.-L. Yang, J.-P. Dou, H. Li, C.-N. Zhang, E. Poem, D. J. Saunders, H. Tang, J. Nunn, I. A. Walmisley, and X.-M. Jin, “A hybrid quantum memory-enabled network at room temperature,” *Sci. Adv.* **6**, eaax1425 (2020).
- [78] D. Tiarks, S. Baur, K. Schneider, S. Dürr, and G. Rempe, “Single-photon transistor using a Förster resonance,” *Phys. Rev. Lett.* **113**, 053602 (2014).
- [79] A. Paris-Mandoki, H. Gorniaczyk, C. Tresp, I. Mirgorodskiy, and S. Hofferberth, “Tailoring Rydberg interactions via Förster resonances: state combinations, hopping and angular dependence,” *J. Phys. B* **49**, 164001 (2016).